



PERGAMON

Available online at [www.sciencedirect.com](http://www.sciencedirect.com)

 ScienceDirect

Acta Astronautica 60 (2007) 141–152

ACTA  
ASTRONAUTICA

[www.elsevier.com/locate/actaastro](http://www.elsevier.com/locate/actaastro)

# Stability of equilibrium points in the restricted full three-body problem

J. Bellerose\*, D.J. Scheeres

*University of Michigan, 1320 Beal Ave., Ann Arbor, MI 48109-2140, USA*

Received 18 May 2005; received in revised form 2 June 2006; accepted 18 July 2006

Available online 24 October 2006

## Abstract

The stability of equilibrium points is investigated for a particle in orbit about a model that mimics a binary asteroid. First, the equations of motion of a particle in the gravitational field of a sphere–ellipsoid system are derived. As in the restricted three-body problem (R3BP), five equilibrium solutions are found. In the R3BP, the stability condition for the equilateral points is given by the Routh criterion. However, in this problem, since the non-spherical mass distribution of one of the primaries is taken into account, stability is a function of the mass ratio, the distance between the bodies and the size parameters of the ellipsoid. Analytic stability criteria for the equilibria are derived and presented for a range of these parameters. In general, although some exceptions exist, it is found that the presence of the ellipsoid body reduces the stability region from the R3BP.

© 2006 Elsevier Ltd. All rights reserved.

*Keywords:* Full two-body problem; Relative equilibria; Restricted full three-body problem; Sphere–ellipsoid system; Equilibrium points; Stability

## 1. Introduction

Over the past few decades, an increasing number of probes have been sent to the small bodies of our solar system. For example, the European Space Agency launched Giotto and Rosetta to comets Halley and 67P/Churyumov-Gerasimenko, respectively, and is continuing their interest with the recently announced Don Quixote mission. The Japanese sent a probe to Halley as well, and are flying the Hayabusa mission (also called Muses-C) that plans to bring a sample of asteroid Itokawa back to Earth in 2010. NASA has had the most number of missions, including the Galileo flybys of asteroids Gaspra and Ida, the NEAR mission to Eros, Deep Space 1 to comet Borrelly and Stardust to comet

P/Wild 2. Additional missions are under development, such as Deep Impact mission to comet Tempel 1 and Dawn to Ceres and Vesta. Generally speaking, the main motivation for the study of small bodies is that they have been minimally processed. Thus, bringing samples back from these worlds will provide important information on the original constituents of our solar system. These small bodies are also of interest for more fundamental studies in orbital dynamics.

Of late there has been an increasing interest in binary asteroids, as it is estimated that they may constitute over 15% of the Near-Earth Asteroid population [1]. There are many important issues of science that can be investigated by studying and sending probes to binary systems. The problem of navigating a spacecraft about them is complex and challenging, as it requires modeling of the asteroid system in addition to the motion of the spacecraft about the system.

\* Corresponding author.

E-mail address: [julielabel@umich.edu](mailto:julielabel@umich.edu) (J. Bellerose).

The problem of binary asteroid orbiters integrates four classical problems of astrodynamics: the Hill problem, the restricted three-body problem, the non-spherical orbiter problem and the full two-body problem (c.f. [2] for a more complete discussion). The Hill problem studies the dynamics of two mutually orbiting bodies which are in orbit about a larger mass, for example the sun. The restricted three-body problem (R3BP) investigates the dynamics of a massless spacecraft in the gravitational field of two spherical or point mass primaries. Finally, the full two-body problem (F2BP) considers the motion of two primaries in orbit about each other where at least one of them has a general, non-spherical mass distribution. The Hill problem and the R3BP have been studied extensively [3]. Stability of equilibrium points has also been studied in the combination of these two problems [4]. Stability in the F2BP has also been recently characterized [5].

In the present work, we investigate the motion of a satellite in the gravitational field of a binary system. The two bodies are modeled as a sphere and a tri-axial ellipsoid and the satellite is assumed to have no influence on the motion of the two primaries. By considering only the motion of the two bodies in orbit about each other, we refer to the F2BP. Two cases can be investigated: the relative equilibria case where the ellipsoid spins at the same rate as its mutual orbit about the sphere, and the more general non-relative equilibrium problem. The F2BP is a current subject of study, especially for the relative equilibria case [5,6]. Having defined the F2BP, we can then study the motion of a satellite in this environment. This particular problem will be referred to as the restricted full three-body problem (RF3BP). The general form of the equations of motion were first derived in [6]. They are further developed in the next section for the case of relative equilibria of the primaries. As in the R3BP, five equilibrium can be found and the stability of the analogue  $L_4$  and  $L_5$  are investigated for two different relative equilibrium configurations. Finally, stability of the F2BP and RF3BP are analyzed and compared.

## 2. Full two-body problem

In order to find the equations of motion of a spacecraft in the vicinity of a binary system, it is necessary to first consider the binary system itself, which we call the F2BP, represented in Fig. 1.

This problem has been investigated in [5] where the equations of motion were posed. They are more convenient to work with when the “sphere restriction” is applied, as shown in Fig. 2. This restriction reduces the problem to lower dimension, as the rotational dynamics

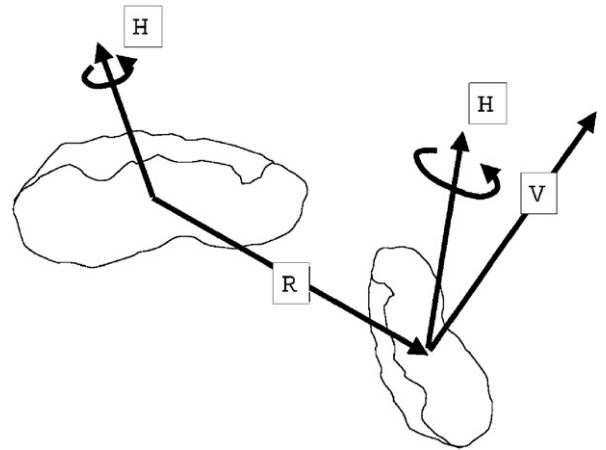


Fig. 1. Representation of the full two-body problem.

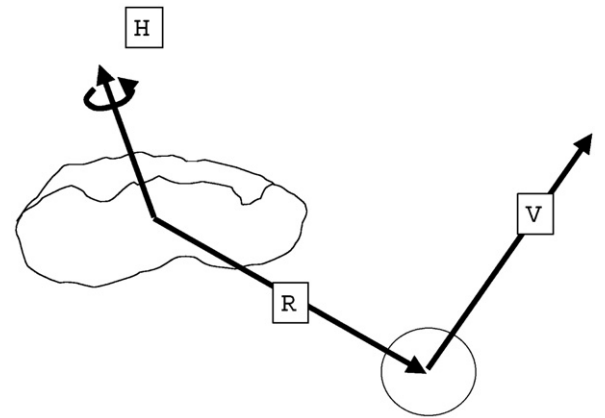


Fig. 2. Representation of the full two-body problem under “sphere restriction”.

of the sphere can be removed while keeping the interesting dynamical features.

In this model,  $M_1$  is the mass of the spherical shape and  $M_2$  is the mass of a general shape. The mass ratio of the two primaries is defined as,

$$v = \frac{M_1}{M_1 + M_2}. \quad (1)$$

The position vector of the sphere relative to the general body is  $\mathbf{r}_b$ . Relative to their center of mass, the positions of the two bodies are,

$$\mathbf{r}_e = -v\mathbf{r}_b, \quad (2)$$

$$\mathbf{r}_s = (1 - v)\mathbf{r}_b, \quad (3)$$

where subscripts  $s$  and  $e$  refer to the sphere and the general body, respectively.

For a rotary coordinate frame fixed to the general body, their relative dynamics are defined by

$$\begin{aligned} \ddot{\mathbf{r}}_b + 2\boldsymbol{\Omega} \times \dot{\mathbf{r}}_b + \dot{\boldsymbol{\Omega}} \times \mathbf{r}_b + \boldsymbol{\Omega} \times (\boldsymbol{\Omega} \times \mathbf{r}_b) \\ = G(M_1 + M_2) \frac{\partial \tilde{U}}{\partial \mathbf{r}_b} \end{aligned} \quad (4)$$

and the rotational dynamics of the general body are described by

$$\hat{\mathbf{I}} \cdot \dot{\boldsymbol{\Omega}} + \boldsymbol{\Omega} \times \hat{\mathbf{I}} \cdot \boldsymbol{\Omega} = -GM_1 \mathbf{r}_b \times \frac{\partial \tilde{U}}{\partial \mathbf{r}_b}, \quad (5)$$

where  $\boldsymbol{\Omega}$  is the angular velocity of the general body,  $\hat{\mathbf{I}}$  is its inertia matrix normalized by its mass and  $\tilde{U}$  is the mutual potential, defined as

$$\tilde{U} = \frac{1}{M_2} \int_{\beta_2} \frac{dm_2(\hat{\boldsymbol{\rho}})}{|\mathbf{r}_b + \hat{\boldsymbol{\rho}}|}, \quad (6)$$

where  $\hat{\boldsymbol{\rho}}$  is the position vector of a mass element of the general body. Note that in the frame fixed to the general body, the mutual potential is time-invariant. This is true independent of whether the system is in relative equilibrium.

To simplify the analysis, the following normalization is introduced. The maximum radius of the distributed body, denoted by  $\alpha$ , and the mean motion of the system at this radius,  $n = \sqrt{G(M_1 + M_2)}/\alpha^3$ , are taken as length and time scales, respectively. Therefore, the normalized position and angular velocity are  $r = r_b/\alpha$  and  $\omega = \Omega/n$ . Eqs. (4) and (5) now become

$$\ddot{\mathbf{r}} + 2\boldsymbol{\omega} \times \dot{\mathbf{r}} + \dot{\boldsymbol{\omega}} \times \mathbf{r} + \boldsymbol{\omega} \times (\boldsymbol{\omega} \times \mathbf{r}) = \frac{\partial U}{\partial \mathbf{r}}, \quad (7)$$

$$\mathbf{I} \cdot \dot{\boldsymbol{\omega}} + \boldsymbol{\omega} \times \mathbf{I} \cdot \boldsymbol{\omega} = -vr \times \frac{\partial U}{\partial \mathbf{r}}. \quad (8)$$

In this case, the potential and inertia are expressed as

$$U = \frac{\alpha}{M_2} \int_{\beta_e} \frac{dm_e(\boldsymbol{\rho})}{|\mathbf{r} + \boldsymbol{\rho}|}, \quad (9)$$

$$\mathbf{I} = -\frac{1}{M_2 \alpha^2} \int_{\beta_e} \tilde{\boldsymbol{\rho}} \cdot \tilde{\boldsymbol{\rho}} dm \quad (10)$$

and are now normalized by the mass.

As discussed in [7], if the distributed body is assumed to have an ellipsoid shape, the general expression for its potential energy is written in terms of elliptic integrals. With the normalization introduced above, the mutual potential can be expressed as,

$$U_e = \frac{3}{4} \int_{\lambda}^{\infty} \phi(\mathbf{r}, v) \frac{dv}{\Delta(v)}, \quad (11)$$

$$\phi(\mathbf{r}, v) = 1 - \frac{x^2}{v+1} - \frac{y^2}{v+\beta^2} - \frac{z^2}{v+\gamma^2}, \quad (12)$$

$$\Delta(v) = \sqrt{(v+1)(v+\beta^2)(v+\gamma^2)}, \quad (13)$$

where  $0 < \gamma \leq \beta \leq 1$  and  $\lambda$  satisfies  $\phi(\mathbf{r}, \lambda) = 0$ . The  $x$ -axis is aligned with the longest axis of the ellipsoid while the  $z$ -axis is along its shortest axis.

The normalized principal moments of inertia are

$$I_{xx} = \frac{1}{5}(\beta^2 + \gamma^2), \quad (14)$$

$$I_{yy} = \frac{1}{5}(1 + \gamma^2), \quad (15)$$

$$I_{zz} = \frac{1}{5}(1 + \beta^2). \quad (16)$$

Relative equilibria are found by setting all velocities to zero in Eqs. (7) and (8). From Eq. (7), we can show that the gravitational acceleration must be perpendicular to the spin axis. With the current symmetry assumption on the gravitational potential, we can also show that the position and gravitational acceleration have to be parallel. With this constraint, Eq. (8) is satisfied if the ellipsoid spins about one of its other principal axes. Note that the spin is parallel to the inertia vector and it is independent of the principal axis the ellipsoid is rotating about [5,6].

Hence, relative equilibria exist when one of the principal axes of the ellipsoid is pointed at the sphere. Then, given a solution along the “ $q$ ”-axis, from Eq. (7) the spin rate is expressed as,

$$\omega^2 = \frac{3}{2} \int_{\lambda}^{\infty} \frac{dv}{(\alpha_q^2 + v)\Delta(v)}. \quad (17)$$

For a general mass distributions, relative equilibria will not necessarily be along a principal axis. A more complete discussion can be found in [8].

For the present problem,  $\alpha_q$  represents the radius along which the sphere is located. Note that here  $\lambda = q^2 - \alpha_q^2$ , where  $q$  is the distance between the primaries, denoted  $r$  in this analysis and along the  $x$ -axis.

The general equilibrium solutions and the relative equilibria of an ellipsoid-sphere system have been studied in [5]. Stability has also been investigated for the two configurations shown in Fig. 3.

For convenience, the conditions for stability of the F2BP are restated below. The characteristic equation was found to be of the form,

$$\zeta^4 + a\zeta^2 + b = 0, \quad (18)$$

where

$$a = 3\omega^2 - U_{rr} - \frac{3}{\Delta(\lambda)} - \sigma(\omega^2 + U_{rr}), \quad (19)$$

$$b = (\omega^2 + U_{rr}) \left[ \frac{3}{\Delta(\lambda)} - \sigma \left( 4\omega^2 - \frac{3}{\Delta(\lambda)} \right) \right], \quad (20)$$

$$\lambda = q^2 - \alpha_q^2. \quad (21)$$

In these expressions,

$$\sigma = \frac{vq^2}{I_{zz}}. \quad (22)$$

For stability to hold, the conditions to satisfy are,

$$a > 0, \quad (23)$$

$$b > 0, \quad (24)$$

$$a^2 - 4b > 0. \quad (25)$$

Ref. [5] provides a more detailed derivation of these stability conditions. Some examples of stability regions are shown in Figs. 4 and 5. These figures show results

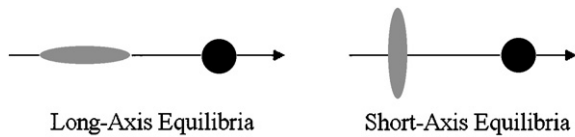


Fig. 3. Configurations investigated for the full two-body problem.

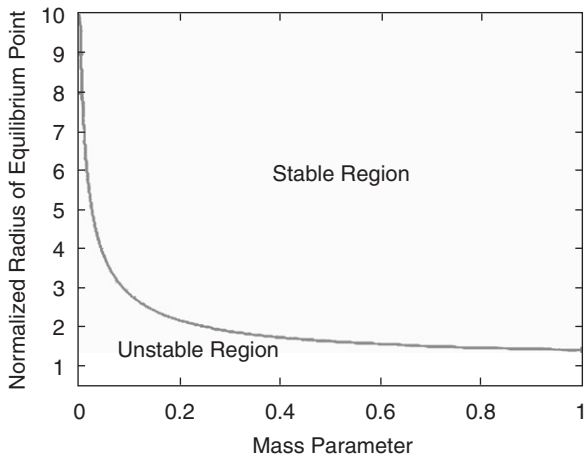


Fig. 4. Stability diagram for planar motion in the long-axis solution. The upper and lower regions denote spectral stability and single hyperbolic manifold instability, respectively [5].

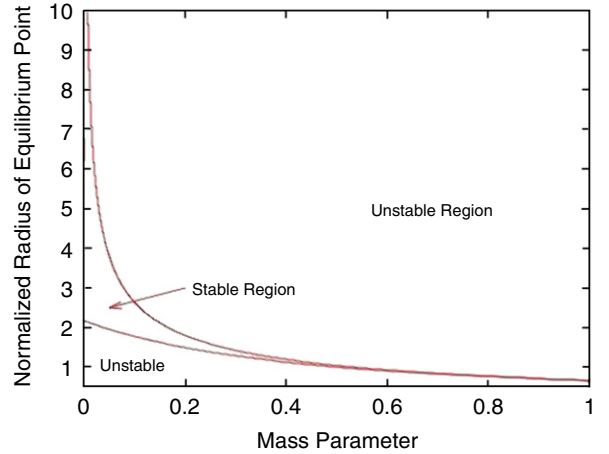


Fig. 5. Stability diagram for planar motion in the short-axis solution. The left, upper and lower regions denote spectral stability, single hyperbolic manifold instability, and spiral manifold instability, respectively [5].

for an ellipsoid with semi-major axes of 1:0.5:0.5. They will be further discussed later and compared with results from the RF3BP.

### 3. Restricted full three-body problem

#### 3.1. Equations of motion of a particle

Having defined the F2BP, we now consider a particle or a spacecraft in the gravitational field of these two bodies. Note that the particle is assumed to have no effect on the motion of the primaries. Since one of them is modeled as an ellipsoid, i.e., its mass distribution is taken into account, we call it the RF3BP.

Let the position of a particle relative to the center of mass of the system denoted as  $\rho$ . As shown in Fig. 6, and assuming relative equilibria, for a particle at a position  $\rho$  from the system's center of mass in a frame rotating with the general body, we find the equations of motion [6],

$$\begin{aligned} \ddot{\rho} + 2\Omega \times \dot{\rho} + \Omega \times (\Omega \times \rho) \\ = G(M_1 + M_2) \frac{\partial \tilde{U}_{12}}{\partial \rho}. \end{aligned} \quad (26)$$

In normalized units, where  $\tilde{\rho} = \rho/\alpha$  is the normalized distance of the particle, Eq. (26) becomes

$$\ddot{\tilde{\rho}} + 2\omega \times \dot{\tilde{\rho}} + \omega \times (\omega \times \tilde{\rho}) = \frac{\partial U_{12}}{\partial \tilde{\rho}}, \quad (27)$$

where  $U_{12}$  is a time-invariant potential energy expression, as the bodies are in mutual equilibrium. It is

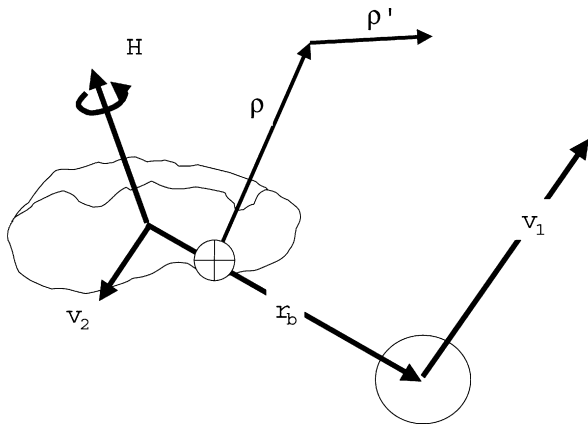


Fig. 6. The restricted full three-body problem.

expressed as,

$$U_{12} = \frac{v}{|\tilde{\rho} - (1-v)r|} + (1-v)U_e(\tilde{\rho} + vr), \quad (28)$$

where  $U_e$  represents the normalized expression for the ellipsoid body and it is defined by Eqs. (11)–(13).

The free parameters of this system are the mass ratio,  $v$ , the distance between the two bodies,  $r$ , and the size parameters of the ellipsoid,  $\beta$  and  $\gamma$ . Given these parameters, the spin rate  $\omega$  is given by Eq. (17).

In the present study, the ellipsoid is assumed to rotate about its maximum moment of inertia along the  $z$ -axis. We first assume that the minimum moment of inertia is aligned with the  $x$ -axis. In this  $x$ - $y$ - $z$  coordinate frame, the corresponding radii are denoted  $\alpha$ ,  $\beta$  and  $\gamma$  where  $0 < \gamma \leq \beta \leq \alpha = 1$ . This configuration is referred as the long-axis configuration.

The equations of motion can be restated in a  $x$ - $y$ - $z$  coordinate system, i.e.,  $\tilde{\rho} = xi + yj + zk$ . The  $x$ ,  $y$  and  $z$  components of Eq. (26) are written as follows:

$$\ddot{x} - 2\omega\dot{y} - \omega^2x = \frac{-v(x - (1-v)r)}{[(x - (1-v)r)^2 + y^2 + z^2]^{3/2}} - (1-v)(x + vr)R_{j\alpha}, \quad (29)$$

$$\ddot{y} + 2\omega\dot{x} - \omega^2y = \frac{-vy}{[(x - (1-v)r)^2 + y^2 + z^2]^{3/2}} - (1-v)(y)R_{j\beta}, \quad (30)$$

$$\ddot{z} = \frac{-vz}{[(x - (1-v)r)^2 + y^2 + z^2]^{3/2}} - (1-v)(z)R_{j\gamma}. \quad (31)$$

The  $R_j$  expressions are elliptic integrals for the mass distribution of the ellipsoid. They are given in the Appendix.

### 3.2. Equilibrium solutions

As for the R3BP, five equilibrium solutions exist. They are shown in Fig. 7.

The three collinear points, along the axis joining the primaries, are unstable in general. However, the two “equilateral points” are of interest as their stability will be affected by the properties of the general body. The equilibrium solutions can be obtained from Eq. (27) by setting all velocities and accelerations to zero

$$\omega \times (\omega \times \tilde{\rho}) = \frac{\partial U_{12}}{\partial \tilde{\rho}}. \quad (32)$$

Hence, the equilibrium solutions are computed from,

$$\omega^2x = \frac{v(x - (1-v)r)}{[(x - (1-v)r)^2 + y^2 + z^2]^{3/2}} + (1-v)(x + vr)R_{j\alpha}, \quad (33)$$

$$\omega^2y = \frac{vy}{[(x - (1-v)r)^2 + y^2 + z^2]^{3/2}} + (1-v)yR_{j\beta}, \quad (34)$$

$$0 = \frac{vz}{[(x - (1-v)r)^2 + y^2 + z^2]^{3/2}} + (1-v)(z)R_{j\gamma}, \quad (35)$$

where  $\omega$  is given by Eq. (17) and the  $R_j$ 's are given in the Appendix.

These algebraic equations were solved numerically in Matlab for varying parameters. Note that  $z = 0$ . By setting  $y = 0$ , we can find solutions for  $x$  corresponding to the three collinear points. As for the R3BP, these points remain unstable as the potential will be a saddle at each point. Since the collinear points are unstable, only the equilateral points were investigated as they can potentially be used for observation and scientific purposes.

For the long-axis configuration, Figs. 8 and 9 show the locations of the analogue equilateral points and their stability as the ellipsoid goes from being spherical to highly oblate and as it becomes massively dominant. The normalized distance is  $r = 1$  and 3, respectively. On these figures, the mass ratio  $v$  varies from 0 to 1 horizontally from left to right and  $\gamma = \beta$  varies from 0 to 1 vertically from bottom to top. These plots have been shifted by  $rv$  and scaled by  $1/r$  so that the ellipsoid is located at the origin and the sphere at a distance of 1 from it. Starred points are stable while dotted ones are unstable.

The effect of the ellipsoid is easily noticed by considering  $v = 0$  (when the ellipsoid is the sole attractor) and  $v = 1$  (when the sphere has all the mass). In the

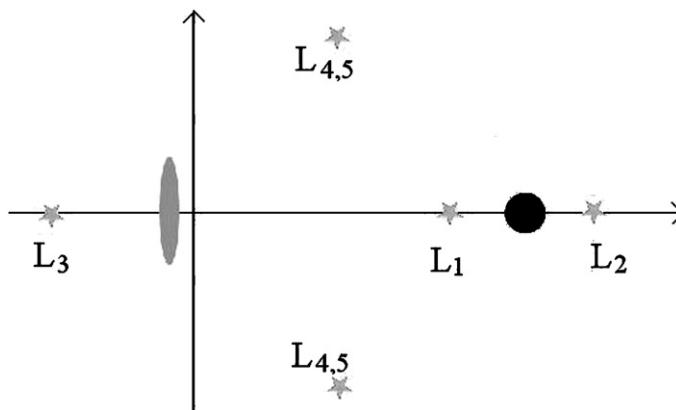


Fig. 7. The analogue Lagrangian points.

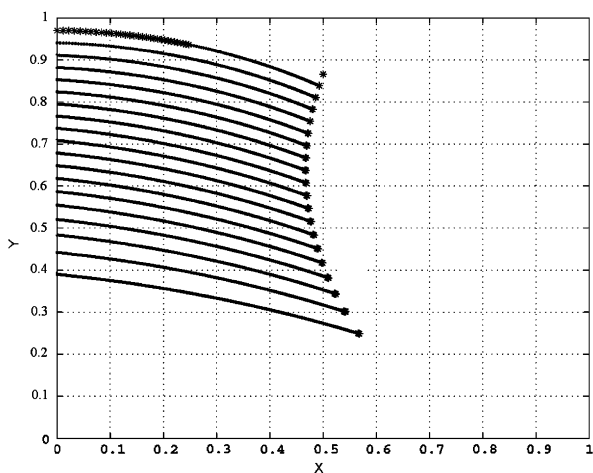


Fig. 8. Locations of the analogue equilibrium points for  $r = 1$  in the  $x$ - $y$  coordinate space for the long-axis configuration. The mass ratio  $v$  varies from 0 to 1 horizontally from left to right and  $\gamma = \beta$  varies from 0 to 1 vertically from bottom to top. Starred points are stable while dotted ones are unstable.

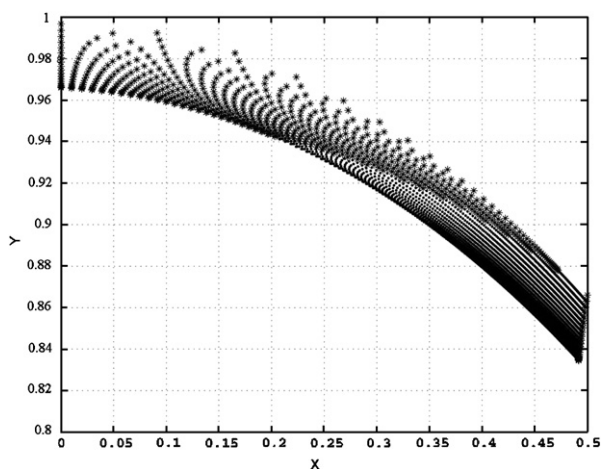


Fig. 9. Locations of the analogue equilibrium points for  $r = 3$  in the  $x$ - $y$  coordinate space for the long-axis configuration. The mass ratio  $v$  varies from 0 to 1 horizontally from left to right and  $\gamma = \beta$  varies from 0 to 1 vertically from bottom to top. Starred points are stable while dotted ones are unstable.

first case, we find the equilibrium solutions lie along the intermediate axis of the ellipsoid. For  $v = 1$  and  $\gamma = \beta = 1$ , the ellipsoid has no effect and we recover the ideal solutions of the R3BP, all points are located at  $x = 0.5$  and  $y = \sqrt{3}/2$  as expected for this shifted system. For  $\gamma = \beta < 1$ , they are not located at the known Lagrangian points as the rotation rate is different than the normal Keplerian rotation rate of the R3BP, due to the non-spherical body.

Similar results were found for the short-axis configuration. They are shown in Figs. 10 and 11 for  $r = 2$  and 3, respectively, with the same normalization as for the long-axis configuration. However, as opposed to this case, the mass ratio  $v$  varies from 0 to 1 horizontally from right to left and  $\gamma = \beta$  varies from 0 to 1 vertically

from top to bottom. For  $v = 0$  and smaller  $\beta$ , the equilibrium points are unstable on the  $y$ -axis. We note that the distribution of the equilibrium points is markedly different for this case, and that the stability intervals are highly constrained. However, as for the long-axis configuration, for  $v = 1$  and  $\gamma = \beta = 1$ , we recover again the solutions of the R3BP.

### 3.3. Stability

For the R3BP, stability of the equilateral points is given by the Routh criteria. The condition to satisfy is

$$v < \frac{1}{2} \left[ 1 - \sqrt{\frac{23}{27}} \right] = 0.0385. \tag{36}$$

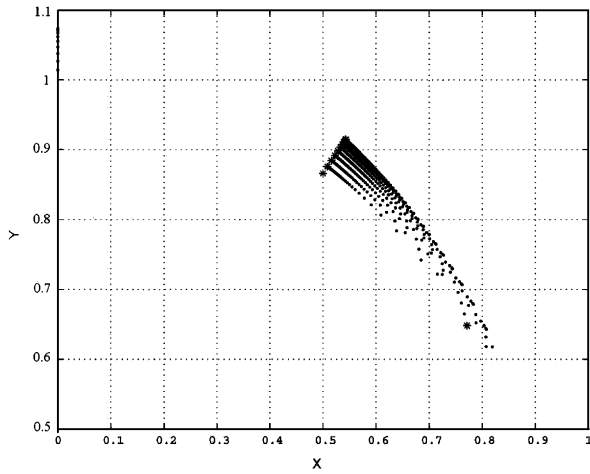


Fig. 10. Locations of the analogue equilibrium points for  $r = 2$  in the  $x$ - $y$  coordinate space for the short-axis configuration. The mass ratio  $\nu$  varies from 0 to 1 horizontally from right to left and  $\gamma = \beta$  varies from 0 to 1 vertically from top to bottom. Starred points are stable while dotted ones are unstable.

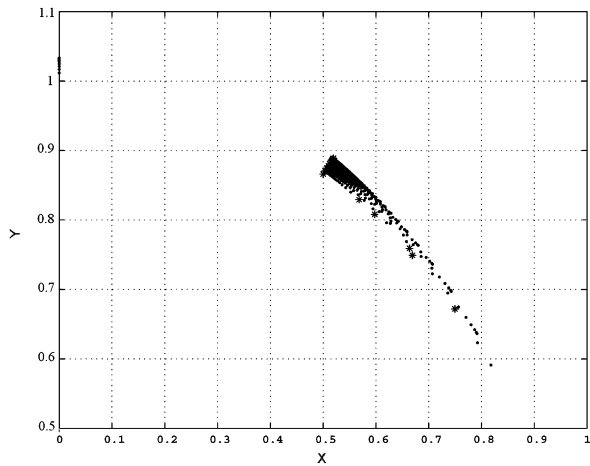


Fig. 11. Locations of the analogue equilibrium points for  $r = 3$  in the  $x$ - $y$  coordinate space for the short-axis configuration. The mass ratio  $\nu$  varies from 0 to 1 horizontally from right to left and  $\gamma = \beta$  varies from 0 to 1 vertically from top to bottom. Starred points are stable while dotted ones are unstable.

Since the mass distribution of the general body is now taken into account, the stability of these locations will be affected by its size and shape and by the distance between the bodies.

In this section, stability is investigated for small deviations from the equilateral position. Introducing  $x = \tilde{x} + dx$  and  $y = \tilde{y} + dy$ , and expanding the potential energy expression, the following equations are derived:

$$\ddot{\tilde{x}} - 2\omega\dot{\tilde{y}} - \omega^2\tilde{x} = \tilde{x}(U_{xxs} + U_{xxe}) + \tilde{y}(U_{xys} + U_{xye}), \quad (37)$$

$$\ddot{\tilde{y}} + 2\omega\dot{\tilde{x}} - \omega^2\tilde{y} = \tilde{y}(U_{yys} + U_{yye}) + \tilde{x}(U_{yxs} + U_{yxe}). \quad (38)$$

The second order partial derivatives were given in [5], for convenience, they are rewritten in the Appendix for the ellipsoid body.

The characteristic equation for the system is found from,

$$\begin{vmatrix} \lambda^2 - \omega^2 - U_{xx} & -2\omega\lambda - U_{xy} \\ 2\omega\lambda - U_{xy} & \lambda^2 - \omega^2 - U_{yy} \end{vmatrix} = 0, \quad (39)$$

where  $U_{xx} = U_{xxs} + U_{xxe}$ ,  $U_{yy} = U_{yys} + U_{yye}$  and  $U_{xy} = U_{xys} + U_{xye}$ .

Expanding the determinant, we find,

$$\lambda^4 + A\lambda^2 + B = 0, \quad (40)$$

where

$$A = 2\omega^2 - U_{xx} - U_{yy} \quad (41)$$

and

$$B = \omega^4 + \omega^2(U_{xx} + U_{yy}) + U_{xx}U_{yy} - U_{xy}^2. \quad (42)$$

For the system to be linearly stable, the following conditions must be satisfied:

$$A > 0, \quad (43)$$

$$B > 0, \quad (44)$$

$$A^2 - 4B > 0. \quad (45)$$

Figs. 12–15 show the stability region associated with the long and short-axis configurations, respectively, as a function of  $\beta$  and  $\nu$ . In Figs. 12 and 13, one parameter has been fixed,  $r = 2$  and  $\gamma/\beta = 1$ , respectively. In the first plot, each line corresponds to different values of  $\gamma/\beta$ , and equal 0.25, 0.5, 0.75 and 1.0. In the second plot, the lines correspond to different values of  $r$ , and equal 2, 3, and 4. Stable regions lie above the lines in the upper figure and below the lines in the lower figure. Figs. 14 and 15 represent the same cases for the short-axis configuration.

It can be seen from these figures that the effect of the ellipsoid is reduced as the distance between the bodies is increased (for large  $r$ ). As  $r$  grows the ellipsoid potential begins to resemble a sphere and the region of stability approaches the Routh criterion for the R3BP, defined by the horizontal dotted line in the plots.

When the ellipsoid dominates, for small  $\nu$ , the region defined by the Routh criterion is much more restricted, especially for small distances between the primaries and small ratios of the intermediate and

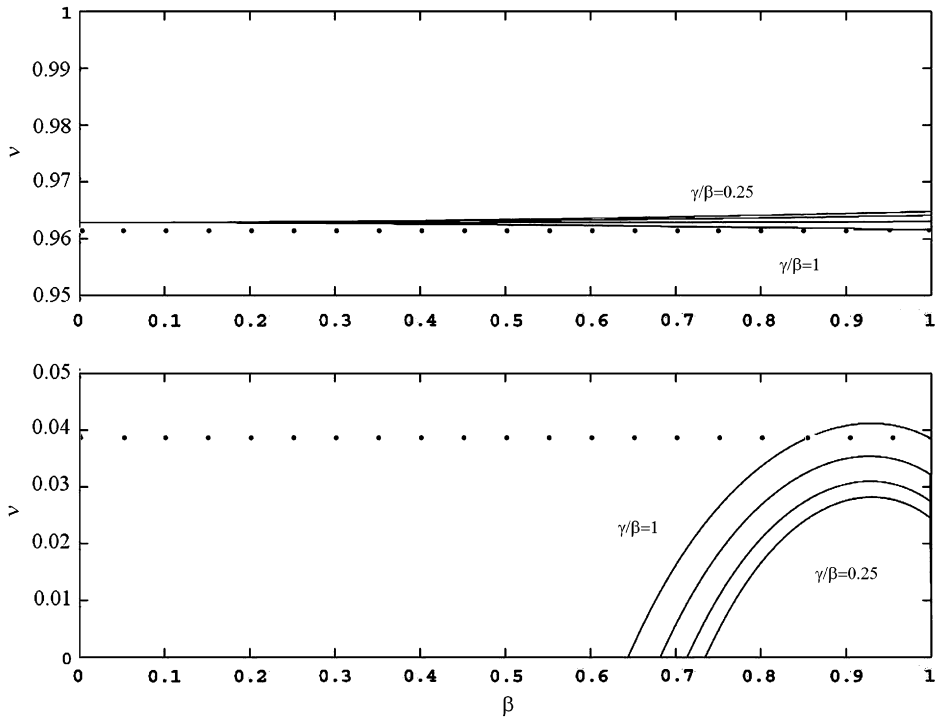


Fig. 12. Stability regions of the long-axis configuration for  $r = 2$  as a function of  $\beta$  and  $\nu$ . Each lines correspond to different values of  $\gamma/\beta$ , and equal 0.25, 0.5, 0.75 and 1.0. Stable regions lie above the lines in the upper figure and below the lines in the lower figure. The horizontal dotted line corresponds to the Routh criterion.

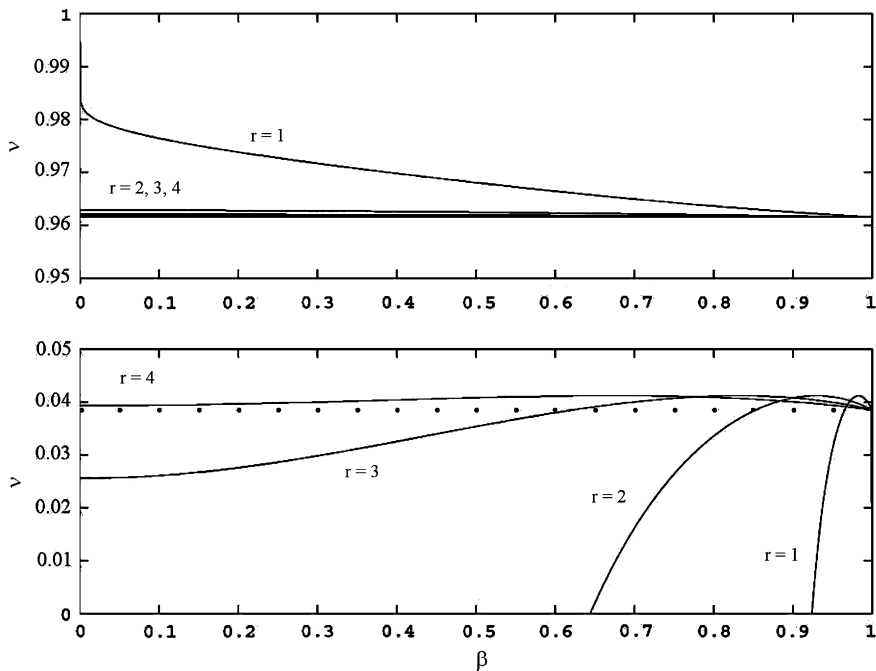


Fig. 13. Stability regions of the long-axis configuration for  $\gamma/\beta = 1$  as a function of  $\beta$  and  $\nu$ . The lines correspond to different values of  $r$ , and equal 2, 3, and 4. Stable regions lie above the lines in the upper figure and below the lines in the lower figure. The horizontal dotted line corresponds to the Routh criterion.

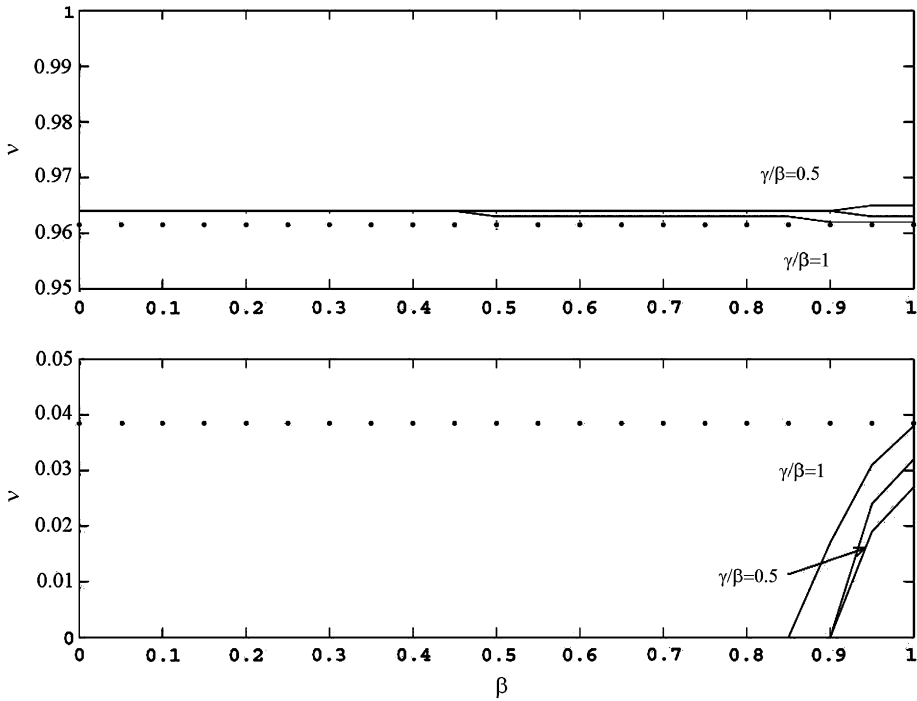


Fig. 14. Stability regions of the short-axis configuration for  $r = 2$  as a function of  $\beta$  and  $\nu$ . Each lines correspond to different values of  $\gamma/\beta$ , and equal 0.5, 0.75 and 1.0. Stable regions lie above the lines in the upper figure and below the lines in the lower figure. The horizontal dotted line corresponds to the Routh criterion.

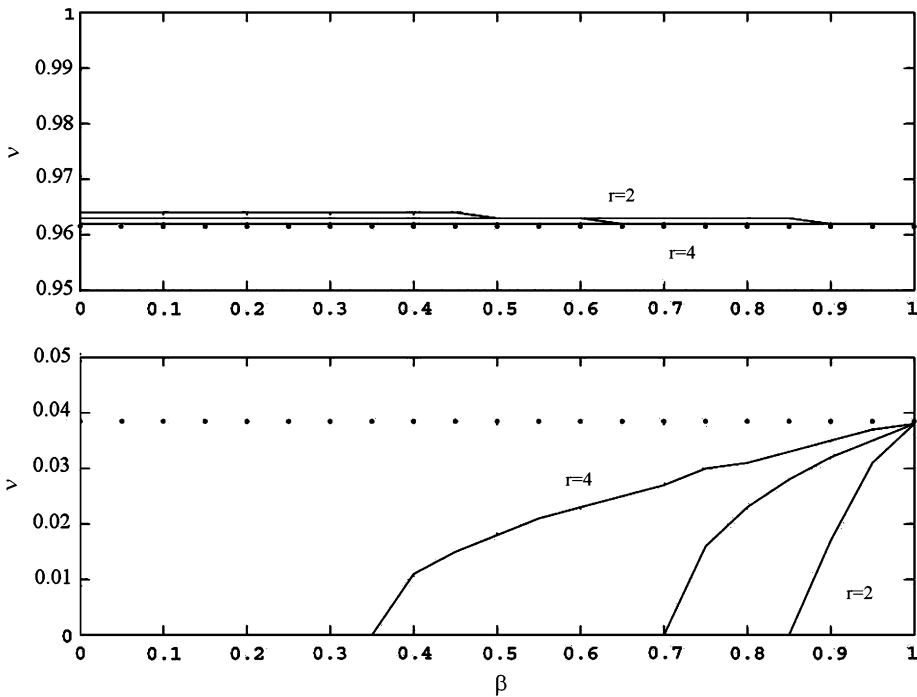


Fig. 15. Stability regions of the short-axis configuration for  $\gamma/\beta = 1$  as a function of  $\beta$  and  $\nu$ . The lines correspond to different values of  $r$ , and equal 2, 3, and 4. Stable regions lie above the lines in the upper figure and below the lines in the lower figure. The horizontal dotted line corresponds to the Routh criterion.

small axis of the ellipsoid. However, for the long-axis configuration, it is interesting to note that the stability limit on the mass ratio is larger than the Routh criterion for some specific values of  $\beta$ . For the short-axis configuration, there is a very small stability region for small  $\nu$ . The stability region is very close, or equal, to the Routh criteria for larger  $\nu$  for all values of  $r$  and size parameters of the ellipsoid. Decreasing  $r$  does not affect the stability region for large  $\nu$ , but it reduces the one for small  $\nu$  and larger values of  $\beta$ . The stability region is also slightly restricted for decreasing  $\gamma/\beta$  for small  $\nu$ .

It is interesting to compare the results from the RF3BP with the stability in the F2BP, i.e., Figs. 4 and 5. These two figures correspond to an ellipse with  $\gamma = \beta = \frac{1}{2}$ . The plots show stability region as function of the mass ratio  $\nu$  and the distance between the bodies,  $r$ . Note that these plots are normalized by the axis of the ellipse aligned with the sphere. For the long-axis configuration, as the distance  $r$  between the bodies increases, the F2BP becomes more and more stable. For the short-axis configuration, the F2BP is usually unstable with some exceptions for small  $\nu$  and large  $r$ .

Stability of both the F2BP and the RF3BP are important and interesting to consider. For the long-axis configuration, we recover the standard R3BP Routh criteria for  $r$  larger than 3 and large mass ratio,  $\nu$ . For small  $\nu$ ,  $r$  needs to be larger than 5 to have both systems stable. For the short-axis case, it seems that stability of both is only possible for small  $\nu$  and  $r$  larger than 5.

This analysis considers the case of relative equilibrium of the F2BP, i.e., synchronized rotation of the ellipsoid–sphere system. Binary systems usually have one of the bodies in synchronized rotation, making the current analysis relevant. In some cases, however, the bodies do not have synchronized motion. Although the analysis for such systems is fundamentally different, the stability results presented above provide insights for this non-equilibrium case. In that particular problem, the triangular points would describe circular motions leading to a time-periodic system at the simplest [9].

#### 4. Conclusions

An analysis of the stability of equilibrium points in the restricted full three-body problem (RF3BP) has been given. It is found that the presence of the ellipsoid body reduces the stability region of the mass ratio  $\nu$  as compared to the R3BP, although there are some exceptions. Equilibrium points in the short-axis configuration reduce the stability regions even more severely.

These results, combined with previous analyses, indicate that it may not be feasible to assume that the equilateral triangle equilibrium point analogues in the RF3BP will be appropriate orbits from which to observe a binary system. While the gravitational models used in this analysis are rather approximate and simplified, it is probable that adding additional realism will tend towards decreasing the stability regions we are interested in. Nonetheless, we plan to study the equivalent regions about a realistic binary asteroid in the future.

In addition to the shape model of the primaries, several assumptions have been made on the dynamics of the system in order to simplify the analysis. For example, in this analysis, the rotation of the ellipsoid was assumed to be synchronized with its mutual orbit about the sphere. The next step would be to investigate the case of non-relative equilibrium, as is sometimes found in nature. Other problems of interest include the computation of periodic orbits in this system and the effects of an elliptic orbit in the full two-body problem.

#### Acknowledgments

This research was funded, in part, by a grant from the Jet Propulsion Laboratory/California Institute of Technology Director's Research and Development Fund. We also thank the "Fonds québécois de la recherche sur la nature et les technologies" of Québec and the Natural Sciences and Engineering Research Council of Canada for their support.

#### Appendix

Originally derived using Ivory's theorem [10], the potential energy expression for an ellipsoid, given the normalization mentioned, is written as

$$U_e = \frac{3}{4} \int_{\lambda}^{\infty} \phi(\mathbf{r}, \nu) \frac{d\nu}{\Delta(\nu)}, \quad (46)$$

$$\phi(\mathbf{r}, \nu) = 1 - \frac{x^2}{\nu + 1} - \frac{y^2}{\nu + \beta^2} - \frac{z^2}{\nu + \gamma^2}, \quad (47)$$

$$\Delta(\nu) = \sqrt{(\nu + 1)(\nu + \beta^2)(\nu + \gamma^2)}, \quad (48)$$

where  $0 < \gamma \leq \beta \leq 1$  and  $\lambda$  satisfies  $\phi(\mathbf{r}, \lambda) = 0$ . The  $x$ -axis is aligned with the longest axis of the ellipsoid while the  $z$ -axis is along its shortest axis.

The first and second order derivatives of the ellipsoid potential are then given by [5],

$$U_x = -\frac{3}{2}x \int_{\lambda}^{\infty} \frac{du}{(u + 1)\Delta(u)}, \quad (49)$$

$$U_y = -\frac{3}{2}y \int_{\lambda}^{\infty} \frac{du}{(u + \beta^2)\Delta(u)}, \tag{50}$$

$$U_z = -\frac{3}{2}z \int_{\lambda}^{\infty} \frac{du}{(u + \gamma^2)\Delta(u)}, \tag{51}$$

$$U_{xx} = -\frac{3}{2} \int_{\lambda}^{\infty} \frac{du}{(u + 1)\Delta(u)} + \frac{3x^2}{(1 + \lambda)^2\Delta(\lambda)} C_L, \tag{52}$$

$$U_{yy} = -\frac{3}{2} \int_{\lambda}^{\infty} \frac{du}{(u + \beta^2)\Delta(u)} + \frac{3y^2}{(\beta^2 + \lambda)^2\Delta(\lambda)} C_L, \tag{53}$$

$$U_{zz} = -\frac{3}{2} \int_{\lambda}^{\infty} \frac{du}{(u + \lambda^2)\Delta(u)} + \frac{3z^2}{(\gamma^2 + \lambda)^2\Delta(\lambda)} C_L, \tag{54}$$

$$U_{xy} = \frac{3xy}{(1 + \lambda)(\beta^2 + \lambda)\Delta(\lambda)} C_L, \tag{55}$$

$$U_{xz} = \frac{3xz}{(1 + \lambda)(\gamma^2 + \lambda)\Delta(\lambda)} C_L, \tag{56}$$

$$U_{yz} = \frac{3yz}{(\gamma^2 + \lambda)(\beta^2 + \lambda)\Delta(\lambda)} C_L. \tag{57}$$

These derivatives are written in terms of the  $R_j$  expressions that are the elliptic integrals representing the mass distribution of the ellipsoid. Using the substitution  $v = u + \lambda$ , they can be solved as written in the following form and can be computed using algorithms from [11],

$$R_{j\alpha} = \frac{3}{2} \int_0^{\infty} \frac{du}{(u + \lambda + 1)\Delta(u + \lambda)}, \tag{58}$$

$$R_{j\beta} = \frac{3}{2} \int_0^{\infty} \frac{du}{(u + \lambda + \beta^2)\Delta(u + \lambda)}, \tag{59}$$

$$R_{j\gamma} = \frac{3}{2} \int_0^{\infty} \frac{du}{(u + \lambda + \gamma^2)\Delta(u + \lambda)}. \tag{60}$$

The short-axis configuration has also been investigated. In this case, the maximum radius of the ellipsoid,  $\alpha$  is aligned with the  $y$ -axis. The  $R_j$  expressions to be used are,

$$R_{j\alpha} = \frac{3}{2} \int_0^{\infty} \frac{du}{(u + \lambda + \beta^2)\Delta(u + \lambda)}, \tag{61}$$

$$R_{j\beta} = \frac{3}{2} \int_0^{\infty} \frac{du}{(u + \lambda + 1)\Delta(u + \lambda)}, \tag{62}$$

$$R_{j\gamma} = \frac{3}{2} \int_0^{\infty} \frac{du}{(u + \lambda + \gamma^2)\Delta(u + \lambda)}. \tag{63}$$

Therefore, using the notation above, the first derivatives are expressed as

$$U_x = -xR_{j\alpha}, \tag{64}$$

$$U_y = -yR_{j\beta}, \tag{65}$$

$$U_z = -zR_{j\gamma}. \tag{66}$$

For the long-axis configuration, the second derivatives of the potential can be expressed as follows:

$$U_{xxe} = (1 - \nu) \left[ -R_{j\alpha} + \frac{x^2}{(1 + \lambda)^2} \times (R_{j\alpha} + R_{j\beta} + R_{j\gamma})C_L \right], \tag{67}$$

$$U_{yye} = (1 - \nu) \left[ -R_{j\beta} + \frac{y^2}{(\beta^2 + \lambda)^2} \times (R_{j\alpha} + R_{j\beta} + R_{j\gamma})C_L \right], \tag{68}$$

$$U_{zze} = (1 - \nu) \left[ -R_{j\gamma} + \frac{z^2}{(\gamma^2 + \lambda)^2} \times (R_{j\alpha} + R_{j\beta} + R_{j\gamma})C_L \right], \tag{69}$$

$$U_{xye} = (1 - \nu) \left[ \frac{xy}{(1 + \lambda)(\beta^2 + \lambda)} \times (R_{j\alpha} + R_{j\beta} + R_{j\gamma})C_L \right], \tag{70}$$

$$U_{xze} = (1 - \nu) \left[ \frac{xz}{(1 + \lambda)(\gamma^2 + \lambda)} \times (R_{j\alpha} + R_{j\beta} + R_{j\gamma})C_L \right], \tag{71}$$

$$U_{yze} = (1 - \nu) \left[ \frac{yz}{(\beta^2 + \lambda)(\gamma^2 + \lambda)} \times (R_{j\alpha} + R_{j\beta} + R_{j\gamma})C_L \right], \tag{72}$$

where

$$C_L = \left[ \frac{1}{(x+vr)^2/(1+\lambda)^2 + y^2/(\beta^2 + \lambda)^2 + z^2/(\gamma^2 + \lambda)^2} \right].$$

For the short-axis configuration, the second derivatives now become

$$U_{xxe} = (1 - \nu) \left[ -R_{j\alpha} + \frac{x^2}{(\beta^2 + \lambda)^2} \times (R_{j\alpha} + R_{j\beta} + R_{j\gamma})C_S \right], \tag{73}$$

$$U_{yye} = (1 - \nu) \left[ -R_{j\beta} + \frac{y^2}{(1 + \lambda)^2} \right. \\ \left. \times (R_{j\alpha} + R_{j\beta} + R_{j\gamma})C_S \right], \quad (74)$$

$$U_{zze} = (1 - \nu) \left[ -R_{j\gamma} + \frac{z^2}{(\gamma^2 + \lambda)^2} \right. \\ \left. \times (R_{j\alpha} + R_{j\beta} + R_{j\gamma})C_S \right], \quad (75)$$

$$U_{xye} = (1 - \nu) \left[ \frac{xy}{(1 + \lambda)(\beta^2 + \lambda)} \right. \\ \left. \times (R_{j\alpha} + R_{j\beta} + R_{j\gamma})C_S \right], \quad (76)$$

$$U_{xze} = (1 - \nu) \left[ \frac{xz}{(\beta^2 + \lambda)(\gamma^2 + \lambda)} \right. \\ \left. \times (R_{j\alpha} + R_{j\beta} + R_{j\gamma})C_S \right], \quad (77)$$

$$U_{yze} = (1 - \nu) \left[ \frac{yz}{(1 + \lambda)(\gamma^2 + \lambda)} \right. \\ \left. \times (R_{j\alpha} + R_{j\beta} + R_{j\gamma})C_S \right], \quad (78)$$

where

$$C_S = \left[ \frac{1}{(x+\nu r)^2/(\beta^2+\lambda)^2 + y^2/(1+\lambda)^2 + z^2/(\gamma^2+\lambda)^2} \right].$$

Note that all the second order partial derivatives should be evaluated at the equilibrium points.

## References

- [1] J.-L. Margot, et al., Binary asteroids in the near-Earth object population, *Science* 296 (5572) (2002) 1445–1448.
- [2] D.J. Scheeres, J. Bellerose, The restricted Hill full 4-body problem: application to spacecraft motion about binary asteroids, invited paper in a special issue of dynamical systems, *An International Journal* 20 (1) (2005) 23–44 (M. Dellnitz and J.E. Marsden (Eds.)).
- [3] V. Szebehely, *Theory of Orbits: The Restricted Problem of Three Bodies*, Academic Press, New York, 1967.
- [4] D.J. Scheeres, The restricted Hill four-body problem with applications to the Earth–Moon–Sun system, *Celestial Mechanics and Dynamical Astronomy* 70 (1998) 75–98.
- [5] D.J. Scheeres, Stability of relative equilibria in the full two-body problem, in: E. Belbruno, D. Folta, P. Gurfil (Eds.), *Astrodynamics, Space Missions, and Chaos*, *Annals of the New York Academy of Science* 1017 (2004) 81–94.
- [6] D.J. Scheeres, S. Augenstein, *Spacecraft Motion about Binary Asteroids*, *Astrodynamics 2003, Part II, Advances in the Astronautical Sciences Series* 116, 991–1010, Univelt, San Diego, AAS Paper 03-564.
- [7] J.M.A. Danby, *Fundamentals of Celestial Mechanics*, second ed., Willmann-Bell, Richmond, VA, 1992.
- [8] D.J. Scheeres, Relative equilibria for general gravity fields in the sphere-restricted full two-body problem, *Celestial Mechanics and Dynamical Astronomy*, accepted for publication.
- [9] J. Bellerose, D.J. Scheeres, Periodic orbits in the vicinity of the equilateral points of the restricted full three-body problem, *AAS/AIAA Conference, Lake Tahoe, 2005*, AAS-05-295.
- [10] F.R. Moulton, *An Introduction to Celestial Mechanics*, Dover, New York, 1970.
- [11] Flannery, et al., *Numerical Recipes in C, The Art of Scientific Computing*, second ed., Press, 1996.